Molecular Crystals and Liquid Crystals

ISSN: 1542-1406 (Print) 1563-5287 (Online) Journal homepage: http://www.tandfonline.com/loi/gmcl20

Nitro Substituted Bisindolylmalimide Derivatives: Position-Dependent Emission

Xiaochuan Li, Nan Zhao, Lihua Yu & Young-A Son

To cite this article: Xiaochuan Li, Nan Zhao, Lihua Yu & Young-A Son (2015) Nitro Substituted Bisindolylmalimide Derivatives: Position-Dependent Emission, Molecular Crystals and Liquid Crystals, 608:1, 273-281, DOI: 10.1080/15421406.2014.940805

To link to this article: http://dx.doi.org/10.1080/15421406.2014.940805

Published online: 03 Mar 2015.

Mol. Cryst. Liq. Cryst., Vol. 608: pp. 273–281, 2015

ISSN: 1542-1406 print/1563-5287 online
DOI: 10.1080/15421406.2014.940805

Nitro Substituted Bisindolylmalimide Derivatives: Position-Dependent Emission

XIAOCHUAN LI,[1,*] NAN ZHAO,[1] LIHUA YU,[1] AND YOUNG-A SON[2,*]

[1]School of Chemistry and Chemical Engineering, Key Lab of Green Chemical Media and Reactions, Ministry of Education, Henan Normal University, China
[2]Department of Advanced Organic Materials Engineering, Chungnam National University, South Korea

A small series of partially alkylated bisindolylmaleimide dyes were prepared containing NO_2 groups at the ortho, meta, *and* para *position. The effect of substitution position in the aryl ring on the photophysical properties of the dyes is discussed in detail. The highly electron withdrawing NO_2 makes different emission behavior of these dyes. Medium quantum yields of fluorescence in toluene solution are observed for derivative with NO_2 substituted in the* ortho *position of aryl ring. Careful analysis of optimized structure and frontier molecular orbitals (HOMO/LUMO) suggests that the electronic rather than steric effect is controlling non-radiative decay.*

Keywords Bisindolylmaleimide; *ortho*, *meta*, and *para* position; photophysical properties; frontier molecule orbitals

Introduction

Small molecules have been act as an attractive area in device fabrication, such as sensors, switches, logical calculation, molecular machines etc [1–4]. Out of various types of small molecular devices with variety of fascination behavior, utilizing fluorescence signal to translate molecular recognition event is the most convenient method.

The benefits of introducing nitro or multiple nitro groups, into organic functional molecules are well documented [5–11]. The prime example is for the field of optical molecules, since the replacement of hydrogen for nitro alternates the electronic properties. Evidently, the highly electron withdrawing nature of nitro affects the electron affinitive nature of the group which it is attached. Moreover, in aromatic rings the number and

This paper was originally submitted to *Molecular Crystals and Liquid Crystals*, Volume 601, Proceedings of the Advanced Display Materials and Devices 2013.

*Address correspondence to Prof. Xiaochuan Li, School of Chemistry and Chemical Engineering, Henan Normal University, East Jianshe Rd. 46, Xinxiang, Henan 453007, China. E-mail: lixiaochuan@henannu.edu.cn

*Address correspondence to Prof. Young-A Son, Department of Advanced Organic Materials Engineering, Chungnam National University, 220 Gung-dong, Daejeon 305-764, Korea. E-mail: yason@cnu.ac.kr

Color versions of one or more of the figures in the article can be found online at www.tandfonline.com/gmcl.

substitution influence the energy of the σ and π frameworks. And also, the energy gap between HOMO and LUMO can be lowered and facilitates electron injection. There is clear precedent that nitro compounds have a benefit over their hydrogen-based counterparts in diverse application.

Bisindoylmaleimide (**BIM**), the core structural framework, is present as the subunit of biologically active metabolites isolated from Streptomycetes, including staurosporine and rebeccamycin. Most aryl or arylamine substituted 3,4-diarylmaleimide derivatives show strong luminescence in solution or in solid state [12–19].

The research focus on photonic applications was emerged in recent decades, which has been demonstrated by the application of **BIM** derivatives as electroluminescent materials [15, 20]. Maleimide is an electron-deficient heterocyclic ring. With electron withdrawing or electro-donor arylamine substituted, the electron distribution in LUMO of **BIM** can be modulated. Based on the chemical modification of **BIM**, photo-physical properties, such as the emission wavelength, Stokes's Shift, and the fluorescence quantum yield in solution or in solid, could be obtained according to the requirement of the designed fluorescent molecules. In this contribution, nitro was introduced to arylamine substituted **BIM**. Our intention was to try and understand the properties through detailed study and structural analysis.

Experimental

Materials

All solvents used in reaction were carefully dried according to the standard procedure and stored over 4Å molecular sieve. All the reagent-grade chemicals were purchased from Aldrich and used without further purification. Melting points were determined on a Mel-Temp® IA9200 digital melting point apparatus in a glass capillary and were uncorrected. All synthesized compounds were routinely checked by TLC, NMR, and Mass. TLC was performed on aluminum-backed silica gel plates (Merck DC. Alufolien Kieselgel 60 F254).

Synthesis

The synthesis of nitroaniline substituted **BIM** was outlined in Scheme 1. **BIM** was obtained by the coupling between dibromomaleimide and 2-methylindole protected by Grignard reagent. The subsequent hydrolysis of **BIM** in aqueous KOH yielded bis-2-methylindolylmaleic acid anhydride. Imidization of bis-2-methyindolemaleic anhydride with nitroaniline yielded the target compound with nitro attaching at different position in the aryl ring.

*General procedure for the synthesis of **1**, **2**, and **3**:*

Bis-2-methylindolylmaleic acid anhydride (50 mg, 0.14 mmol), nitroaniline (39.5 mg, 0.16 mmol) dissolved in 25 mL THF. Potassium carbonate (10 mg) was added to the above solution and heated to reflux for about 24 h. The reaction process was monitored by TLC. The reaction was quenched until the bis-2-methylindolylmaleic acid anhydride was disappeared on TLC. After cooling to room temperature, the reaction mixture was poured to water (25 mL) and the organic phase was separated. Aqueous was extracted with ethyl acetate (3×25 mL). The collected organic phase was dried over $MgSO_4$. After separation of $MgSO_4$, the organic solvent was evaporated in vacuum. Crude product was purified by silica gel column chromatography with dichloromethane/petroleum ether (20:1) as the eluant, affording dark red solid.

Counpound **1**: 25 mg, Yield 37%; red powder; mp: 298–301°C; ^{1}H NMR (400 MHz, DMSO–d_6): δ 11.42 (2H, s), 8.23–8.21 (1H, d, $J = 8$ Hz), 7.98–7.94 (1H, t, $J = 7.6$ Hz),

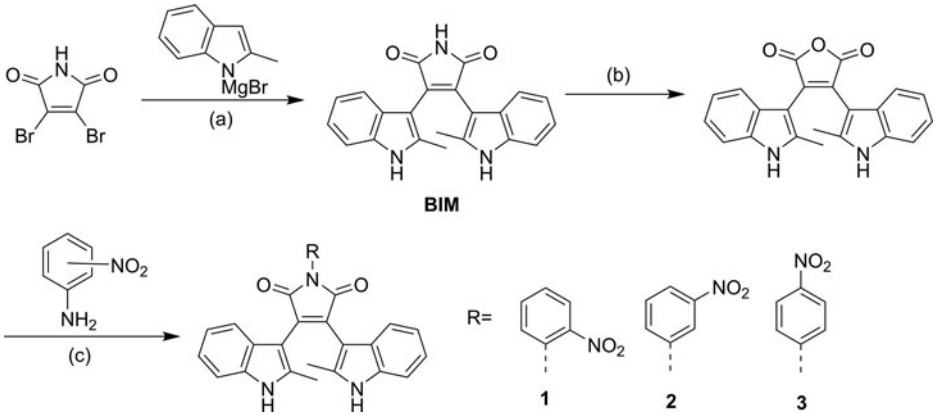

Scheme 1. Synthetic route and conditions: (a) toluene/Et_2O/THF (5:1:1), refl. 24h; (b) 10% aq. KOH, refl. 40 min; (c) 2N HCl; (d) $CH_3OCH_2CH_2OH$, refl. 24h.

7.89–7.87 (1H, d, $J = 7.60$ Hz), 7.76–7.72 (1H, t, $J = 8.0$ Hz), 7.28–7.26 (2H, d, $J = 8.0$ Hz), 7.05 (2H, s), 7.01–6.97 (2H, t, $J = 7.2$ Hz), 6.81–6.77 (2H, dd, $J = 7.6, 7.2$ Hz), 2.03 (s, 6H); ^{13}C NMR (100 MHz, DMSO–d_6): δ 169.5, 145.6, 138.5, 136.0, 134.9, 132.1, 131.5, 129.9, 126.9, 126.1, 125.9, 121.5, 119.8, 119.7, 111.2, 103.5, 13.5; MS (EI, 70 eV) m/z 476 (M^+); HRMS: calcd for $C_{28}H_{20}N_4O_4$: 476.1485, found 476.1481.

Counpound **2**: 40 mg, Yield 60%; red powder; mp: 285–288°C; ^{1}H NMR (400 MHz, DMSO–d_6): δ 11.38 (2H, s, NH), 8.52 (1H, s,), 8.27–8.25 (1H, d, $J = 8.0$ Hz), 8.10–8.08 (1H, d, $J = 7.6$ Hz), 7.86–7.82 (1H, dd, $J = 8.4, 8.0$ Hz), 7.27–7.25 (4H, m), 7.01–6.97 (2H, t, $J = 7.6$ Hz), 6.81–6.78 (2H, dd, $J = 7.6, 6.8$ Hz), 2.04 (6H, s); ^{13}C NMR (100 MHz, DMSO-d_6): δ 169.0, 147.4, 135.1, 133.1, 132.4, 130.9, 129.7, 126.1, 121.3, 120.6, 119.1, 118.9, 110.3, 102.7, 12.5; MS (EI, 70 eV) m/z 476 (M^+); HRMS: calcd for $C_{28}H_{20}N_4O_4$: 476.1485, found 476.1488.

Counpound **3**: 65 mg, Yield 97%; red powder; mp: 300–303°C; ^{1}H NMR (400 MHz, DMSO–d_6): δ 11.40 (2H, s), 8.42–8.40 (2H, d, $J = 9.2$ Hz), 7.92–7.90 (2H, d, $J = 9.2$ Hz), 7.26–7.24 (2H, d, $J = 8.0$ Hz), 7.16 (2H, s), 6.70–6.96 (2H, t, $J = 7.2$ Hz), 6.80–6.77 (2H, dd, $J = 7.6, 7.2$ Hz), 2.03 (6H,s); ^{13}C NMR (100 MHz, DMSO-d_6): δ 168.7, 144.8, 138.1, 135.1, 130.9, 126.1, 123.7, 120.5, 119.2, 118.8, 110.3, 102.7, 12.7; MS (EI, 70 eV) m/z 476 (M^+); HRMS: calcd for $C_{28}H_{20}N_4O_4$: 476.1485, found 476.1487.

Measurements

^{1}H and ^{13}C NMR Spectroscopy

^{1}H and ^{13}C nuclear magnetic resonance (NMR) spectra were recorded on a Brucker AM-400 spectrometer operating at frequencies of 400 MHz for proton and 100 MHz for carbon in DMSO-d_6. Proton chemical shifts (δ) are relative to tetramethylsilane (TMS, $\delta = 0$) as internal standard and expressed in parts per million. Spin multiplicities are given as *s* (singlet), *d* (doublet), *t* (triplet), and *m* (multiplet) as well as *b* (broad). Coupling constants (*J*) are given in Hertz.

Mass and High Resolution Mass Spectra (HRMS)

Mass spectra measured on a LC-MS (Waters UPLC-TQD) mass spectrometer. High resolution mass spectra (HRMS) were measured on Brucker microOTOF II Focus instrument.

UV-Vis and Emission Spectra

Absorption spectra were measured with a PERSEE TU-1900 and an Agilent 8453 spectrophotometer. Emission spectra were measured with a Shimadzu RF-5301PC fluorescence spectrophotometer. Solvents used in photochemical measurement were spectroscopic grade and were purified by distillation. The stock solution of compounds (2×10^{-3} M) was prepared in THF, and a fixed amount of these concentrated solutions were added to each experimental solution. All the experiments were done repeatedly, and reproducible results were obtained. Prior to the spectroscopic measurements, solutions were deoxygenated by bubbling nitrogen through them.

Quantum Yield

The Φ_F values in solution were measured following a general method with quinine sulphate ($\Phi = 0.55$ in 50 mM H_2SO_4 solution) as a standard. Dilute solutions of compounds in THF were used. Sample solution was in quartz cuvettes and degassed for ~15 min. The degassed solution has absorbance of 0.05–0.09 at absorbance maxima. The fluorescence spectra were recorded 3-4 times and average value of integrated areas of fluorescence was used for the calculation of Φ_F in solution. The refractive indices of solvents at the sodium D line were used.

Theoretical Calculations

For the theoretical study of excited state phtophysics of **1**-**3**, the *DMol*[3] program packaged in *Material Studio* was used. The ground state geometries and the frontier molecular orbital of the compound were calculated using the density function theory (DFT) with the B3LYP hybrid functional and the double numerical plus *d*-functions (DND) atomic orbital basis set.

Results and Discussion

The target compounds **1**, **2**, and **3** were synthesized by conventional condensation and purified rigorously to remove spurious fluorescent impurities. The compounds were characterized by standard analytical techniques including ^{1}H, ^{13}C NMR spectroscopies, mass spectrometry and melting points. All data were fully consistent with the proposed structures. The ambient temperature electronic absorption spectra for the derivatives were recorded in dilute THF. Profiles for **1**, **2**, and **3** are shown in Figure 1. Similar absorption characteristics were observed between **1**, **2**, and **3**. The typical electronic transition locate around 445-500 nm with a broad shoulder 350–445 nm, which can be assigned to $\pi-\pi^*$ transitions from the S_0 to S_1 and S_2 states. Different substituent pattern for nitro in aryl ring does not result in a significant difference in the UV–vis spectrum with respect to **BIM** and its derivatives [18, 19]. Similar contour were observed for **1**, **2**, and **3** in nonpolar solvents such as toluene and dioxane and in polar solvents such as chloroform, ethanol, and DMF.

The emission profiles were recorded in various solvents and shown in figure 2. 2 and 3 are fluorescent in fluid toluene and dioxane solution at room temperature. In contrast, the *ortho*-NO_2 derivatives **3** exhibited very weak emission in toluene and dioxane with respect to that of **2** and **3**. Emission peaks for **1**-3 are almost identical to each other with a difference of several nano meters. However, there is large difference in the emission intensity among **1**-**3** in toluene. The *meta*-NO_2 derivative **2** shows strong and medium emission in toluene and dioxane and relatively weak emission in other solvents. The quantum yields (Φ) of **2**

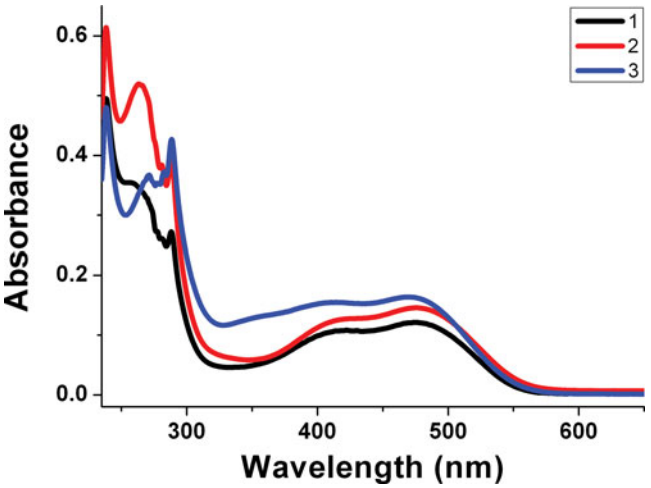

Figure 1. Ambient temperature absorption of **1**, **2**, and **3** (1.0×10^{-5} M) (black solid = **1**, red solid = **2**, blue solid = **3**) recorded in THF.

in toluene and dioxane were estimated to be 0.31 and 0.17, respectively. Emission of **3** in toluene is medium with the quantum yield of 0.18. In other solvents, emission of **3** is weak. Almost in most of the solvents, emission of **1** is weak. By comparison of all the emission data collected, the *ortho* substitution pattern for nitro quench the emission significantly but there is no obvious overall trend for their emission behavior with increasing the polarity of solvents.

To gain further insight into the geometrical, electronic, and optical properties of **1**-**3**, computational study using Material Studio. The energy-minimized structure was precisely refinement using DFT based on B3LYP/DND basis set. No higher level of calculation was deemed necessary, considering the purpose was to compare properties of the molecules. The energy-minimized structures for **1-3** are collected in Figure 3. It is noted that for each structure the aryl group is orthogonal to the imide plane, owing to the unfavorable steric interactions between the ring and the two flanking oxygen of imide. The calculated electrostatic potentials for **1**-**3** are shown in Figure 3. Not surprisingly, the two electron withdrawing carbonyl polarizes the electrostatic potential at their position. When compared to basic **BIM**, the introduction of nitro to the *meta*- and *para*- position distorts the electron distribution in the aryl ring.

The size and signs of the highest occupied molecular orbital (HOMO) and lowest unoccupied molecular orbital (LUMO) are illustrated in Fig. 4. The subtle difference between these compounds is best appreciated by comparison of the frontier molecular orbitals. For all the cases, the overall appearance of HOMO is similar, with the HOMO residing primarily on the bisindolylmaleimide units and little electron density located at the benzene ring. For **1**, the electron density of the LUMO delocalize away to the nitro unit significantly and partly to imide and benzene ring. However, the electron distribution trend of LUMO for **2** and **3** is different from **1**. For **2**, and **3**, the LUMO locate on the imide ring mainly. Only a small part of the electron density spread over the pyrrole ring. The *meta* or *para* substitution pattern for nitro does not affect the electron distribution trend of **BIM** derivatives [19]. The stronger electron withdrawing effect of *ortho*-NO_2 substitution disturbed the electron density distribution significantly and moved it to nitro

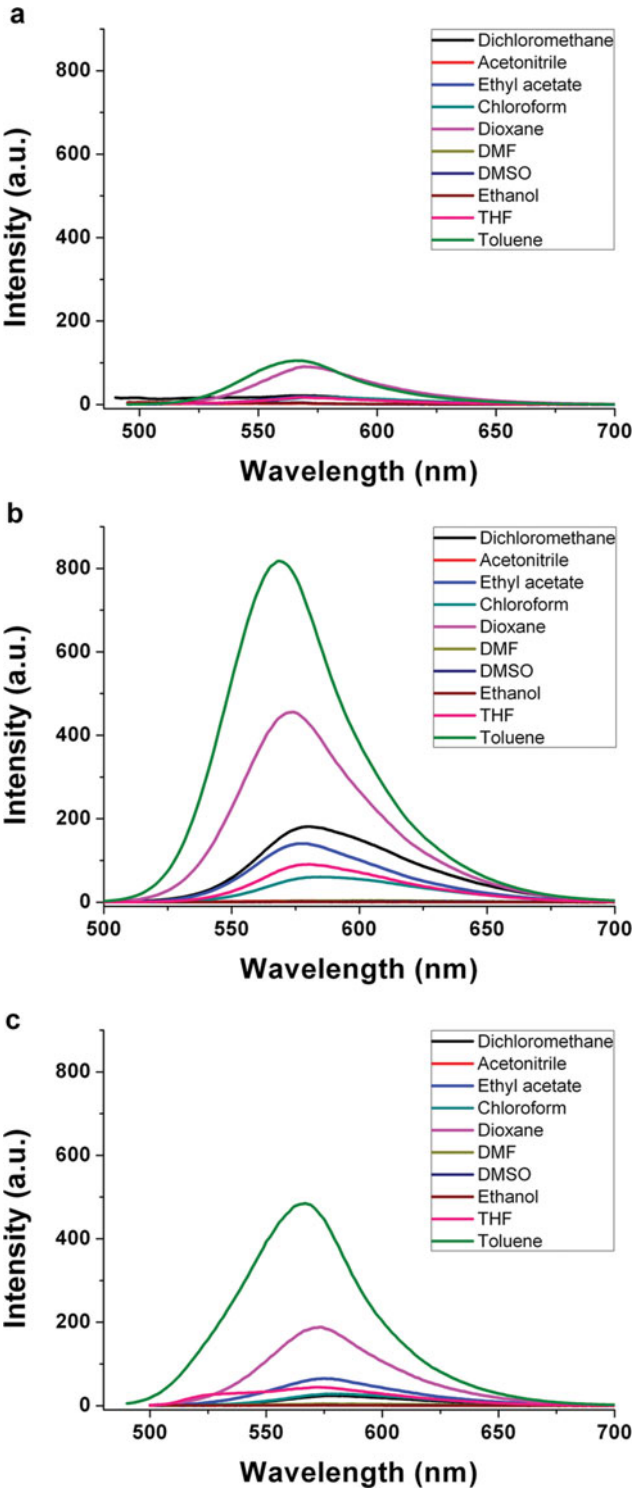

Figure 2. Ambient temperature emission spectra of **1**, **2**, and **3** (1.0×10^{-5} M) recorded in various solvents.

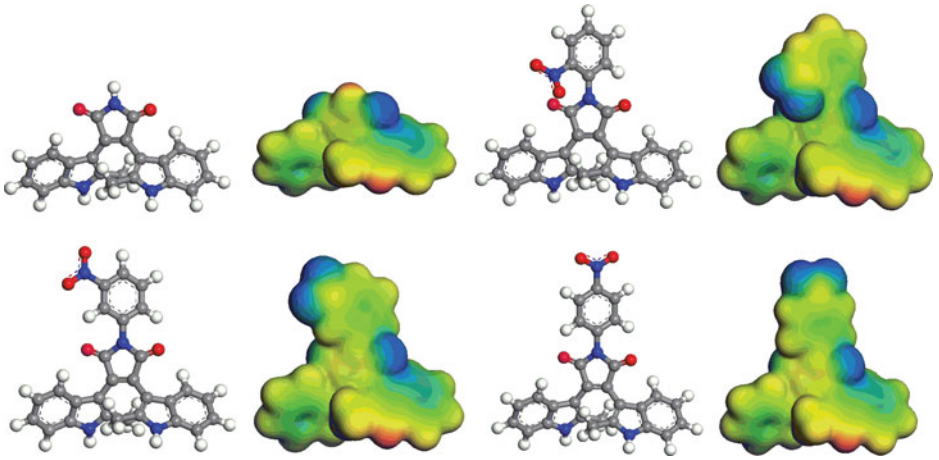

Figure 3. Illustrations of the total electrostatic potential mapped onto the isosurface of the molecular orbital for the **BIM** derivatives. *Note*: the more negative the value of the potential the more blue the color.

and aryl ring, supporting effect of photo-induced electron and excitation energy transfer in **1** and thus quenching the fluorescence emission. Such delocalization also results in an increase in the energy difference between HOMO/LUMO levels. It is also noticeable that the electronic effect of *ortho*-NO_2 shifted the HOMO/LUMO levels higher than that of *meta* and *para* derivatives. This could be attributed to larger steric repulsion between nitro and carbonyl of imide, preventing rotation around the C–N bond. Due to the intramolecular repulsion between NO_2-benzene ring and imide ring, twist conformation lead noncoplanar

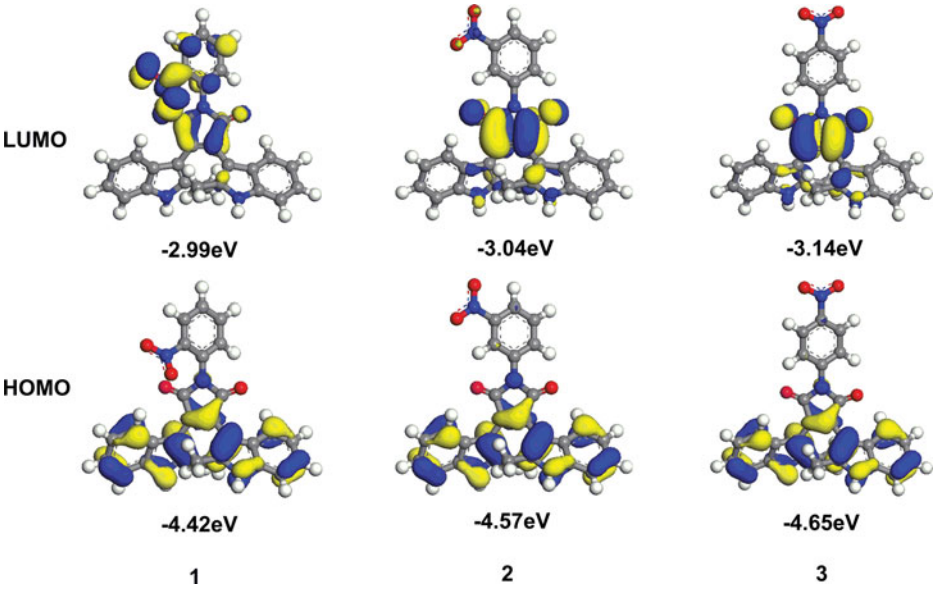

Figure 4. Electron density distributions and energies of the frontier orbitals of **1**, **2**, and **3**.

arrangements of **1**, **2**, and **3**. The angles between imide ring and benzene ring were calculated to be 49.4, 39.8, and 37.5°, respectively. Obviously, the torsion angle follows the order **3** < **2** < **1**. It is easy to understand that the Φ is greater for **2** and **3** than **1** in toluene. In addition, the electron withdrawing effect of *para* position is stronger than that of *meta* position, which results $\Phi_2 < \Phi_3$. It would appear that an electronic rather than a steric effect is controlling non-radiative decay.

Conclusion

We have designed and synthesized three **BIM** derivatives with highly electro withdrawing groups, nitro, attached at the *ortho*, *meta*, and *para* position. Fully characterization was carried out by NMR and MS. Investigation of absorption and emission shows that *meta* and *para* position derivatives (**2** and **3**) are fluorescent in toluene with the quantum yield of 0.31 and 0.18, respectively. However, the ortho derivative (**1**) is dark in most of the nonpolar and polar solvents. Computational study in energy-minimized structure and frontier molecular orbitals uncover the different photophysical properties in theory. The *para* nitro substitution pattern perturbed the LUMO distribution on imide ring significantly than that of *meta* and *para* substitution pattern. That is to say orbital contribution of LUMO is significant at the ortho site with electron withdrawing group attached. Very subtle *ortho* electronic effect, together with part of steric effect, play an important role in designing functionalized **BIM** derivatives. The *meta*-NO_2-phenyl and *para*-NO_2-phenyl units appear to interesting candidates, and we expect to prepare and study such compounds in the near future.

Funding

This work was supported by the National Natural Science Foundation of China (grant no. 21072048 and 21272060). This research was supported by the Basic Science Research Program through the National Research Foundation of Korea (NRF) funded by the Ministry of Education, Science and Technology (grant no. 2013054767).

References

[1] Oh, J., & Hong, J.-In. (2013). *Org. Lett.*, *15*, 916.
[2] Okuno, K., Shigeta, Y., Kishi, R., & Nakano, M. (2013). *J. Phys. Chem. Lett.*, *4*, 2418.
[3] Chen, S., Guo, Z., Zhu, S., Shi, W.-E., & Zhu, W. (2013). *ACS Appl. Mater. Interfaces*, *5*, 5623.
[4] Ismail, A. I., Mantha, J. H., Kim, H. J., Bell, T. W., & Cline, J. I. (2011). *J. Phys. Chem. A*, *115*, 419.
[5] Lusic, H., Uprety, R., & Deiters, A. (2010). *Org. Lett.*, *12*, 916.
[6] Haiser, K., Koller, F. O., Huber, M., Regner, N., Schrader, T. E., Schreier, W. J., & Zinth, W. (2011). *J. Phys. Chem. A*, *115*, 2169.
[7] Thottempudi, V., & Shreeve, J. M. (2011). *J. Am. Chem. Soc.*, *133*, 19982.
[8] Schwartz, K. R., Chitta, R., Bohnsack, J. N., Ceckanowicz, D. J., Miro, P., Cramer, C. J., & Mann, K. R. (2012). *Inorg. Chem.*, *51*, 5082.
[9] Su, W., Zhou, Y., Ma, Y., Wang, L., Zhang, Z., Rui, C., Duan, H., & Qin, Z. (2012). *J. Agric. Food Chem.*, *60*, 5028.
[10] Nandi, L. G., Facin, F., Marini, V. G., Zimmermann, L. M., Giusti, L. A., Da Silva, R., Caramori, G. F., & Machado, V. G. (2012). *J. Org. Chem.*, *77*, 10668.
[11] Zhou, L., Stewart, G., Rideau, E., Westwood, N. J., & Smith, T. K. (2013). *J. Med. Chem.*, *56*, 796.
[12] Yeh, H.-C., Wu, W.-C., & Chen, C.-T. (2003). *Chem. Commun.*, 404.

[13] Wu, W.-C., Yeh, H.-C., Chan, L.-H., & Chen, C.-T. (2002). *Adv. Mater.*, *14*, 1072.
[14] Chen, C.-T. (2004). *Chem. Mater.*, *16*, 4389.
[15] Chan, L.-H., Lee, Y.-D., & Chen, C.-T. (2006). *Macromolecules*, *39*, 3262.
[16] Yeh, H.-C., Chan, L.-H., Wu, W.-C., & Chen, C.-T. (2004). *J. Mater. Chem.*, *14*, 1293.
[17] Yeh, H.-C., Wu, W.-C., Wen, Y.-S., Dai, D.-C., Wang, J.-K., & Chen, C.-T. (2004). *J. Org. Chem.*, *69*, 6455.
[18] Li, X., Chen, J., Ma, D., Zhang, Q., & Tian, H. (2005). *Proc. of SPIE*, *5632*, 357.
[19] Li, X., Xu, Y., Wang, B., & Son, Y.-A. (2012). *Tetrahedron Lett.*, *53*, 1098.
[20] Chiu, C.-W., Chow, T. J., Chuen, C.-H., Lin, H.-M., & Tao, Y.-T. (2003). *Chem. Mater.*, *15*, 4527.